Simulations of a hydrogen-filled capillary discharge waveguide

N. A. Bobrova,[1] A. A. Esaulov,[1,2] J.-I. Sakai,[2] P. V. Sasorov,[1] D. J. Spence,[3] A. Butler,[3] S. M. Hooker,[3] and S. V. Bulanov[4]
[1]*Institute for Theoretical and Experimental Physics, Bol'shaya Cheremushkinskaya Street 25, 117259 Moscow, Russia*
[2]*Laboratory for Plasma Astrophysics, Toyama University, 3190 Gofuku, Toyama 930-8555, Japan*
[3]*Department of Physics, University of Oxford, Oxford OX1 3PU, United Kingdom*
[4]*General Physics Institute of the Russian Academy of Sciences, Vavilov Street 38, 117942 Moscow, Russia*
(Received 2 May 2001; published 17 December 2001)

A one-dimensional dissipative magnetohydrodynamics code is used to investigate the discharge dynamics of a waveguide for high-intensity laser pulses: the gas-filled capillary discharge waveguide. Simulations are performed for the conditions of a recent experimental measurement of the electron density profile in hydrogen-filled capillaries [D. J. Spence *et al.*, Phys. Rev. E **63**, 015401 (R) (2001)], and are found to be in good agreement with those results. The evolution of the discharge in this device is found to be substantially different to that found in *Z*-pinch capillary discharges, owing to the fact that the plasma pressure is always much higher than the magnetic pressure. Three stages of the capillary discharge are identified. During the last of these the distribution of plasma inside the capillary is determined by the balance between ohmic heating, and cooling due to electron heat conduction. A simple analytical model of the discharge during the final stage is presented, and shown to be in good agreement with the magnetohydrodynamic simulations.

DOI: 10.1103/PhysRevE.65.016407 PACS number(s): 52.65.Kj, 52.38.Hb, 52.80.Tn, 42.55.Vc

I. INTRODUCTION

A number of important applications, such as short-wavelength lasers and schemes for particle acceleration, involve the interaction with plasmas of ultrashort laser pulses with peak intensities in the range 10^{16-21} W cm^{-2} [1–4]. The laser-plasma interaction length achieved in such applications is fundamentally limited by diffraction to distances of order the Rayleigh range, and in practice is often further restricted by refraction of the propagating laser pulse.

In order to increase the distance over which the intensity of the laser pulse is maintained at a value close to that at its focus, it is necessary to channel the laser pulse in some manner [5]. A wide variety of methods for channelling intense laser pulses has been investigated, including relativistic and ponderomotive channelling [6,7], guiding by grazing-incidence reflection from the walls of a hollow capillary [8–10], and plasma waveguides. In this last method, a plasma is formed with a transverse electron density profile with a minimum on the axis of propagation. An electron density profile of this form corresponds to a transverse refractive index profile that decreases with radius, providing a focusing effect that can counteract diffraction and refraction. A number of techniques for generating a plasma waveguide have been studied, including, hydrodynamic expansion of a laser-produced cylindrical spark [11–13], ionization of gas by a hollow Bessel beam [14], and a several types of capillary discharge [15–22].

Capillary discharges are an attractive method for forming a plasma waveguide since they require no auxiliary laser, can be scaled to long lengths, and, for some types, offer long device lifetimes. Three quite distinct varieties of capillary discharge have been used to generate plasma waveguides. Discharge-ablated capillary waveguides [15–17,20] operate by ablation and ionization of the wall of an initially evacuated capillary to form a plasma with a radial profile suitable for guiding [23,24]. Capillary discharges with much greater current densities, typically peak currents of several tens of kA in a pulse of tens of nanosecond duration, are able to form a plasma channel by the pinch effect. This type of capillary discharge can be operated in either initially-evacuated capillaries, or gas-filled capillaries, and the channel may be formed either in the initial compression phase of the discharge [18,19], or after reflection of the shockwave at the capillary axis when the plasma is in dynamical and thermal equilibrium with the walls of the capillary [25–27].

Recently a third type of capillary discharge waveguide has been demonstrated: the gas-filled capillary discharge waveguide [22]. In this device, a current pulse is passed through a capillary with an inner diameter of a few hundred microns, prefilled with gas at a pressure of tens to hundreds of millibar. The current pulse has a peak of a few hundred amperes, and a duration of order 200 ns. Measurements of the transverse electron density profile in a hydrogen-filled device have shown that a parabolic plasma channel is indeed formed [22]. Furthermore, recently a H-filled capillary discharge waveguide was used to guide laser pulses with peak intensities of greater than 10^{16} W/cm^2, through 20- and 40-mm long capillaries with pulse energy transmissions of 90% and 80%, respectively [28].

Gas-filled capillary discharge waveguides offer a number of advantages for guiding intense laser pulses, such as low transmission and coupling losses, the ability continuously to tune the plasma pressure, and a long device lifetime. In addition, for H-filled capillaries the plasma channel may be fully ionized, which minimizes spectral or temporal distortion of the guided laser pulse. In order to assist the development of this waveguide, it is important to understand the mechanisms by which the guiding electron density profile is formed. In the present paper we present the results of magnetohydrodynamic simulations of the plasma dynamics of a hydrogen-filled capillary discharge waveguide. The model employed was modified from one that has previously been used to investigate *Z*-pinch discharges suitable for x-ray la-

sers and waveguides for high-intensity laser pulses [25–27,29–31,20].

The magnetohydrodynamics (MHD) simulations are compared with measurements [22] of the electron density profile in a hydrogen-filled capillary discharge waveguide, and good agreement is found. The simulations show clearly that the mechanism of formation of the guiding electron density profile is very different from that which occurs in *Z*-pinch capillary discharge waveguides.

II. BASIC EQUATIONS

We investigate the discharge dynamics in a capillary prefilled by nonionized gas. During the discharge, gas ionization occurs as a result of the increasing electron temperature, so that the discharge plasma consists of neutral and ionized components. In the parameter range under consideration, it is important to describe the following dissipative processes: electron and ion thermal conductivities, Joule heating, Nernst and Ettinghausen effects, radiation losses, and viscosity. It is also important to incorporate the degree of ionization into both the equation of state and the dissipative coefficients. We use the approximation of two-temperature (ion and electron), one-fluid magnetohydrodynamics.

Owing to the large length-to-radius ratio of the capillary ($l/R_0 \gg 1$, where l and R_0 are the length and a radius of the capillary, respectively) a one-dimensional approximation is considered in which all the values depend only on radius r and time t. We note that in one-dimensional approximation we take into account all dissipative processes. The relevant MHD equations read

$$\frac{\partial \rho}{\partial t}+\frac{1}{r}\frac{\partial}{\partial r}(r\rho v)=0, \tag{1}$$

$$\rho\left(\frac{\partial v}{\partial t}+v\frac{\partial v}{\partial r}\right)=-\frac{\partial p}{\partial r}-\frac{1}{c}jB-\frac{\partial}{\partial r}\Pi_{rr} -\frac{1}{r}(\Pi_{rr}-\Pi_{\varphi\varphi}), \tag{2}$$

$$\frac{\partial}{\partial t}\left(\frac{B}{\rho r}\right)+v\frac{\partial}{\partial r}\left(\frac{B}{\rho r}\right)=\frac{c}{\rho r}\frac{\partial}{\partial r}E, \tag{3}$$

$$\rho\left(\frac{\partial \varepsilon_e}{\partial t}+v\frac{\partial \varepsilon_e}{\partial r}\right)+\frac{p_e}{r}\frac{\partial}{\partial r}(rv)=jE-\frac{1}{r}\frac{\partial}{\partial r}(rq_e)-Q_r +C_{ei}(T_i-T_e), \tag{4}$$

$$\rho\left(\frac{\partial \varepsilon_i}{\partial t}+v\frac{\partial \varepsilon_i}{\partial r}\right)+\frac{p_i}{r}\frac{\partial}{\partial r}(rv) =-\frac{1}{r}\frac{\partial}{\partial r}(rq_i)+C_{ei}(T_e-T_i)-\Pi_{rr}\frac{1}{r}\frac{\partial}{\partial r}(rv) -\frac{v}{r}(\Pi_{\varphi\varphi}-\Pi_{rr}). \tag{5}$$

Here ρ is the plasma density, $p=p_e+p_i$ the plasma pressure (being the sum of the electron and ion pressures), v the radial component of the plasma velocity, B the azimuthal component of the magnetic field, Π_{ik} the ion viscous stress tensor, E the axial component of the electric field in the comoving frame in which the plasma is locally at rest, ε_e and ε_i the internal energies of the electron and ion components of the plasma, related to the unit of the plasma mass, C_{ei} the rate of thermal transfer between ions and electrons, and T_e and T_i the electron and ion temperatures, respectively, $j=(c/4\pi r)\partial(Br)/\partial r$ the axial component of the electric current density, q_e and q_i the radial components of the electron and ion heat fluxes, and Q_r the rate of radiative energy loss per unit of volume. The ion component of the plasma is assumed to be unmagnetized, so for the nonzero components of the ion viscosity tensor Π_{ik} we have

$$\Pi_{rr}=\frac{2}{3}\eta_0\left(\frac{v}{r}-2\frac{\partial v}{\partial r}\right), \tag{6}$$

$$\Pi_{\varphi\varphi}=\frac{2}{3}\eta_0 r^2\frac{\partial}{\partial r}\frac{v}{r^2}. \tag{7}$$

We take full account of all dissipative effects in the plasma electron component. In this case we write the generalized Ohm's law in the form

$$E=\frac{j}{\sigma_\perp}-\mathcal{N}B\frac{\partial T_e}{\partial r}, \tag{8}$$

$$q_e=-\kappa_{e\perp}\frac{\partial T_e}{\partial r}+\mathcal{N}BT_e j. \tag{9}$$

The second terms on the right-hand side of Eqs. (8) and (9) describe the so-called Nernst and Ettinghausen effects, respectively. The ion heat flux is given by

$$q_i=-\kappa_{i\perp}\frac{\partial T_i}{\partial r}. \tag{10}$$

The expressions for the thermal conductivity $\kappa_{e\perp}$, the Nernst coefficient $\mathcal{N}$, the electric conductivity $\sigma_\perp$, ion viscosity η_0, and the rate of thermal transfer between ions and electrons are taken from Ref. [32], where the well-known system of the Braginskii equations [33] was generalized for the case of a plasma with a large mean value of the ion charge and the possible considerable difference between the Coulomb logarithms for electron-electron and electron-ion collisions was taken into account

$$\kappa_{e\perp}=\frac{n_e T_e}{m_e\nu_{ei}}\Gamma_1(x_e,w), \quad \mathcal{N}=-\frac{1}{m_e c\,\nu_{ei}}\Gamma_4(x_e,w), \tag{11}$$

$$\sigma_\perp=\frac{e^2 n_e}{m_e\nu_{ei}}[1-\Gamma_5(x_e,w)]^{-1}, \tag{12}$$

$$C_{ei}=3\frac{m_e}{Am_A}n_e\nu_{ei}, \quad \eta_0=0.96n_i T_i\nu_{ii}^{-1}, \tag{13}$$

where n_e and n_i are the electron and ion densities, e and m_e are the charge and mass of the electron, respectively, A is the atomic number of the element of interest, m_A is the atomic unit of mass. The parameter $x_e=\omega_{Be}/\nu_{ei}$ is large if the electrons are strongly magnetized, and is small if the influence of the magnetic field upon the dissipative coefficients is negligible. The Lorentz parameter, $w=\lambda_{ee}/(\sqrt{2}z\lambda_{ei})$, characterizes the relative role of electron-electron and electron-ion collisions, and the $\Gamma_i(x_e,w)$ are the functions defined in Ref. [32] and are of the order of 1 in the case under consideration. The electron-ion and ion-ion collision frequencies are written as follows:

$$\nu_{ei}=\frac{4\sqrt{2\pi}e^4z_1^2n_i\lambda_{ei}}{3\sqrt{m_e}T_e^{3/2}},\quad \nu_{ii}=\frac{4\sqrt{\pi}e^4z_1^4n_i\lambda_{ii}}{3\sqrt{Am_A}T_i^{3/2}}, \tag{14}$$

where z is the mean ion charge, $z_1=z$ for $z\geqslant 1$ and $z_1=1$ for $z<1$, and λ_{ii} is the Coulomb logarithm for ion-ion collisions. In dense, ionized plasmas there is a considerable difference between the Coulomb logarithms for electron-electron, electron-ion, and ion-ion collisions. For the parameters typical of gas-filled capillary discharges, the classical description of the process of Coulomb collisions is sufficient, and we use the following expressions:

$$\lambda_{ee}=\frac{1}{2}\ln\frac{9T_e^3}{16\pi e^6n_e}, \tag{15}$$

$$\lambda_{ei}=\frac{1}{2}\ln\frac{9T_e^3}{4\pi z_1^2e^6n_e(1+z_1T_e/T_i)}, \tag{16}$$

$$\lambda_{ii}=\frac{1}{2}\ln\frac{9T_i^2T_e}{16\pi z_1^4e^6n_e(1+z_1T_e/T_i)}. \tag{17}$$

At low temperatures, as long as the mean ion charge is considerably less than unity, there is a noticeable fraction of neutral particles in the plasma. We renormalize the electron-ion collision frequency ν_{ei} by taking into account the contribution of neutral particles to the electron scattering. Thus all dissipative coefficients are defined by expressions in which the electron-ion collision frequency is substituted by the effective collision frequency involving the contribution from neutral atoms (see Ref. [34]). These expressions have been applied to both a highly ionized plasma and a plasma with a low degree of ionization. This procedure provides a qualitatively accurate and universal description of limiting cases corresponding to strongly ionized and weakly ionized plasmas, as well as to the intermediate cases.

The model description of the equation of state and the ionization degree has been elaborated and used for simulation of capillary discharges and dense Z pinches in plasmas with arbitrary atomic number of the element of interest Z and the degree of ionization z (see, for example Refs. [25,29,34]). But the case of the hydrogen-filled capillary discharge waveguide, that is a plasma consisting of free ideal electrons and nonideal gas of atoms and singly-ionized ions, has not been considered previously. This we do below.

The model described above is used for both the hydrogen filling the capillary and for the capillary wall material. The approximation of local thermodynamic equilibrium is used separately for the electron and ion components. For the free energy of ideal free electrons, neutral atoms, and singly ionized ions we have

$$\begin{aligned}F(V,T_e,T_i,z)=z\chi_0&-zT_e\left\{1+\ln\left[\left(\frac{m_eT_e}{2\pi\hbar^2}\right)^{3/2}\frac{2V}{z}\right]\right\}\\&-zT_i\left\{1+\ln\left[\left(\frac{Am_AT_i}{2\pi\hbar^2}\right)^{3/2}\frac{2V}{z}\right]\right\}\\&-(1-z)T_i\left\{1+\ln\left[\left(\frac{Am_AT_i}{2\pi\hbar^2}\right)^{3/2}\frac{V}{1-z}\right]\right\}\\&+\frac{\mathcal{E}_0}{6}\left[2+\left(\frac{\mathcal{V}_0}{V}\right)^3-3\frac{\mathcal{V}_0}{V}\right].\end{aligned} \tag{18}$$

Here χ_0 is the ionization potential of the neutral atom, $V=Am_A/\rho$ is specific volume of the atomic cell, and z is the degree of ionization or the mean ion charge. The first term on the right-hand side of Eq. (18) describes the energy of ionization, whereas the next three terms are the sum of free energies of ideal gases of electrons, ions, and atoms. The last term on the right-hand side of Eq. (18) describes the nonideal correction to the free energy of a gas of atoms. We use the simplest form of the nonideal equation of state. It takes into account the phase transition from condensed matter to atomic gas, but neglects all phase transitions in the condensed phase and all processes of aggregation (disassociation) of atoms into molecules. The specific heat capacity c_v is chosen to be constant. The free energy of ions tends to the free energy of an ideal ion gas when $\rho\to 0$. The parameter $\mathcal{V}_0=Am_A/\rho_0$ is related to the density, ρ_0, of the condensed material at zero external pressure and at zero temperature. The parameter $\mathcal{E}_0$ is related to the energy per atom of full sublimation and dissociation to separate atoms at $T=0$, which is equal to $\mathcal{E}_0/3$. Hydrodynamic ablation of the wall material starts at about $T_i\approx T_s=3^{-3/2}\mathcal{E}_0$. However, for the present case the final lattice temperature appears to be much less than T_s, and as such the exact form of the equation of state at $T_i\sim T_s$ is unimportant. In the case of Al_2O_3 ceramics $A\approx 20$, $\rho_0\approx 3.5$ g/cm^3, $\mathcal{E}_0$ is assumed to be about 4 eV. For the hydrogen, $\mathcal{E}_0$ and $\mathcal{V}_0$ are chosen to be sufficiently small that the nonideal corrections to the hydrogen equation of state are negligible.

Equation (18) gives all necessary thermodynamic functions. The equilibrium state of ionization, z, corresponds to the minimum free energy at given T_e, T_i, and V

$$\left(\frac{\partial F}{\partial z}\right)_{V,T_e,T_i}=0. \tag{19}$$

Equation (19) generalizes the Saha equation for a plasma composed of atoms and singly ionized ions to the case when $T_i\neq T_e$.

For the ion (lattice) thermal conductivity we write the interpolation formula

$$\kappa_i = 3.9 \frac{3}{4\sqrt{\pi}} \frac{T_i^{5/2}}{z_i^4 e^4 \Lambda_{ii} m_i} + g \frac{\mathcal{E}_0}{T_i} \frac{\rho}{\rho_0}, \tag{20}$$

which describes the contributions from plasma and lattice thermal conductivities. The factor $\mathcal{E}_0/T_i$ in the second term in Eq. (20) is found from the theory of thermal conductivity of dielectrics for temperature above the Debye temperature [35]. The factor ρ/ρ_0 is introduced to suppress the contribution of the second term in Eq. (20) in the plasma region. Here the constant g is chosen for the thermal conductivity of alumina to be approximately equal to the experimental value at the relevant temperatures [36]. Thus $g\,(\mathcal{E}_0/T_{100}) = 25$ $\mathrm{Wm}^{-1}\,\mathrm{K}^{-1}$, where $T_{100} = 373$ K corresponds to 100 °C.

For the radiation energy losses we have used the approximation formula, which takes into account bremsstrahlung and recombination radiation [37]. However, the influence of radiation cooling on plasma dynamics when the magnitude of the electric current is significantly less than the Pease-Braginskii current value [38,39] is negligibly small, as is the case for the H-filled capillary discharge under consideration.

The physical model described in this section or its modifications have been used to simulate the dynamics of dense *Z* pinches [40–42] and both discharge-ablated [27,29,31] and *Z*-pinch capillary discharges [25,26,29,30,34]. In all cases the simulations showed good agreement with experimental results [31,30,41,42], and we conclude that the model adopted is adequate. For the computer simulations we used the MHD code PICA [26,34].

Initial and boundary conditions

The capillary is taken to be prefilled with nonionized gas of uniform density and temperature. The discharge is initiated by a pulse of current driven by an external circuit. The total electric current through the discharge, $I(t)$, including that which flows through the capillary wall, may be considered to be a given function of time. We parametrize the total discharge current in the form,

$$I(t) = I_0 \Phi\left(\frac{\pi t}{t_0}\right), \tag{21}$$

where the function $\Phi(\pi t/t_0)$ is determined by the external electric circuit, I_0 is the peak current and t_0 is an effective half-width of the electric current pulse.

III. RESULTS OF MHD SIMULATIONS

We have used the physical model described above to simulate the discharge under the conditions of the recent experiment to measure the electron density in a H-filled capillary discharge [22]. In that work the capillary was formed from alumina, with an inner diameter of 300 μm. The discharge current pulse was approximately sinusoidal, with a half-period of approximately 200 ns and a peak of 250 A. The initial hydrogen pressure in the capillary was measured to be 67 mbar at room temperature.

For the simulations we consider an alumina capillary with $R_0 = 150$ μm, prefilled with pure hydrogen of uniform density and temperature at an initial density of 5.6×10^{-6} g/cm^3. For $t > 0$ the current pulse is taken to be described by $I(t) = I_0 \sin(\pi t/t_0)$, where $I_0 = 250$ A, and $t_0 = 200$ ns. Initially, there is no electric current inside the channel, and hence in order to initiate the discharge, the hydrogen is assumed to be slightly ionized ($T_e = 0.3$ eV) at $t = 0$. The initial breakdown of the discharge, which lasts about 10 ns, cannot be described by Eqs. (1)–(5) because, as is well known, the breakdown exhibits three-dimensional structure. In addition, the effects of plasma nonquasineutrality are important. However, the initial stage is short compared with the full time of the discharge and it does not substantially affect the plasma parameters at later times.

Figure 1 (color) presents quantitative information about the temporal evolution of the calculated radial distribution of plasma parameters inside the channel. The first frame of Fig. 1 shows an (r,t) diagram of the trajectories of fluid elements in the MHD simulation. The second and the third frames show the distribution in the (r,t) plane of the electron density and temperature, respectively, and the fourth frame shows the distribution of the degree of ionization.

The general properties of the discharge can be described as follows. After the breakdown the current pulse heats the plasma and creates an azimuthal component of the magnetic field. However, pinching of the plasma is negligibly weak since the plasma pressure is much higher than the magnetic field pressure. The maximum plasma pressure is found to be approximately 46 bar. The plasma is confined from expansion in the radial direction by the elasticity and the inertia of the capillary walls. We do not see the propagation of a compression wave from the capillary wall to the channel axis, in contrast to the existence of such a compression wave for gas-filled capillaries operated at higher current densities [25,26,29,30].

In detail, there are three stages of plasma evolution inside the capillary. The first stage lasts approximately 50 ns, during which the radial distributions of the electron density, temperature, and the degree of ionization remain homogeneous. As the electric current increases n_e, T_e, and z grow with time up to the moment of almost full ionization of hydrogen at $t \approx 55$ ns ($z =$ 0.85, 0.95, and 0.99 at $t = 50$, 55, and 60 ns, respectively). The characteristic time of the penetration of electric field in plasma, the skin time $t_\sigma = 4\pi\sigma_\perp R_0^2/c^2$, is of the order of 1 ns. As a result, the radial distribution of the electric field is homogeneous and consequently the electric current penetrates the plasma very quickly, and plasma is heated and ionized locally. The plasma parameter $\beta = 8\pi(p_e + p_i)/B^2$, which characterizes the relative contribution of the magnetic pressure, is of the order of 100. As such the plasma pressure is much greater than the magnetic pressure, and as a result there is no pinch effect.

The situation changes significantly at the time of almost complete ionization of plasma, which occurs when $T_e \approx 2$ eV. The redistribution of plasma across the capillary

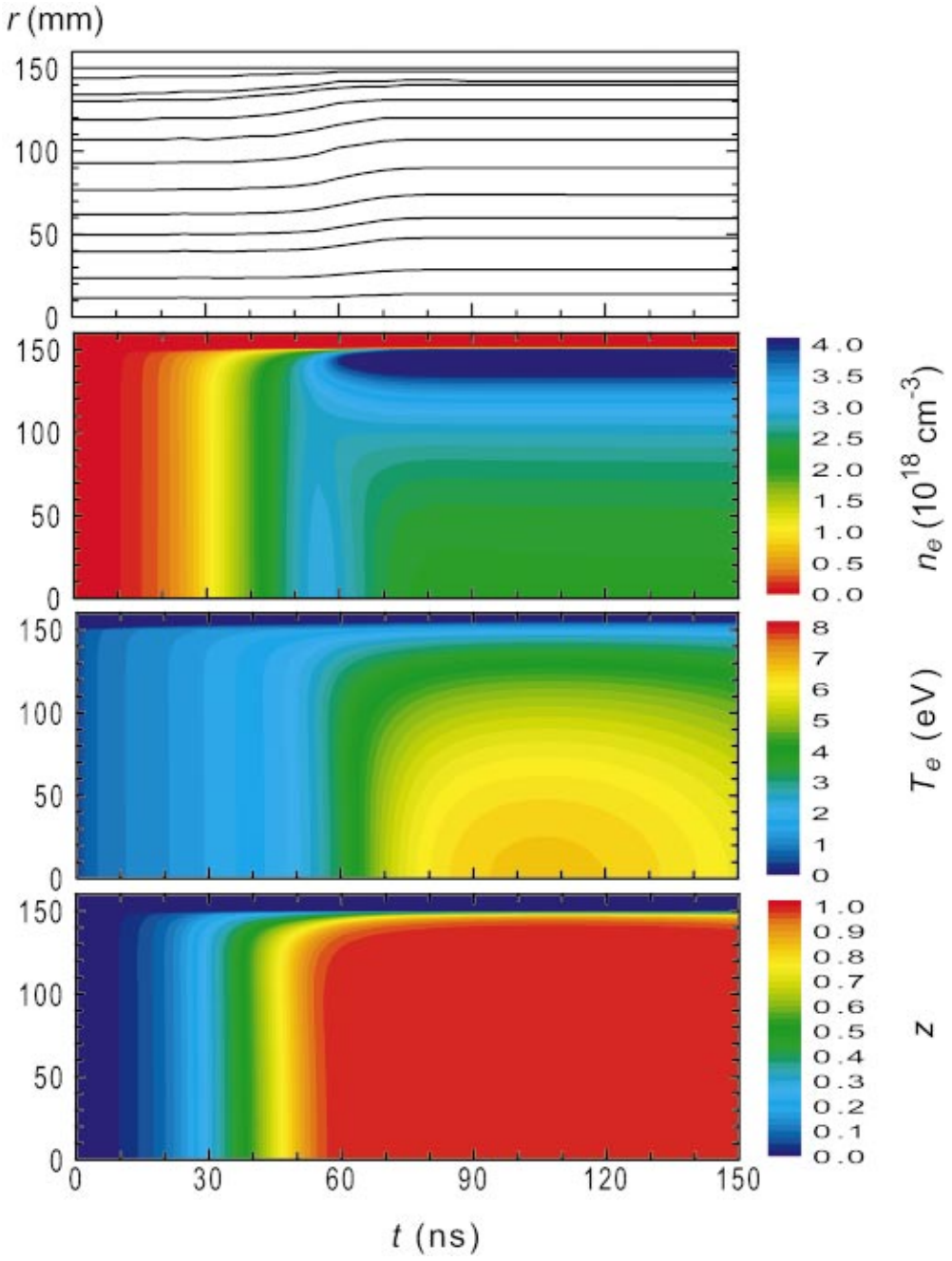

FIG. 1. (Color) Results of computer simulation of capillary discharge dynamics for an alumina capillary of 300 μm inner diameter prefilled with 67.0 mbar of pure hydrogen. The current pulse is taken to be sinusoidal with a peak value $I_0=250$ A and half-period time $t_0=200$ ns. The first frame shows the (r,t) diagram of the trajectories of hydrogen plasma elements. The second and the third frames show the distributions in the (r,t) plane of electron density in units of 10^{18} cm^{-3} and temperature in units of eV, respectively. The fourth frame shows the distribution of the degree of ionization of hydrogen. The scales on the right-hand side of the figures show values of electron density, temperature, and the degree of ionization of hydrogen, respectively.

channel is clearly seen in Fig. 1 during the interval $t=50-80$ ns. The rising electric current leads to an increase of plasma temperature and heat flux due to thermal conduction. During this phase of the discharge the thermal conduction time, $t_\chi = R_0^2 c_v/\kappa_{e\perp}$, decreases and becomes comparable to, and subsequently less than, the characteristic time of the electric discharge. The skin time remains of the same order as in the first stage of the discharge. The plasma pressure is homogeneous, but the plasma radial distribution of temperature is inhomogeneous since the plasma is cooled near the wall. Hence during this second stage of plasma evolution thermal conduction becomes significant.

During the third stage of the discharge the plasma remains almost immobile in the radial direction. For $t \gtrsim 80$ ns the acoustic (~ 5 ns), thermal conduction (~ 10 ns), and skin (~ 2 ns) times are much less than the discharge time. For

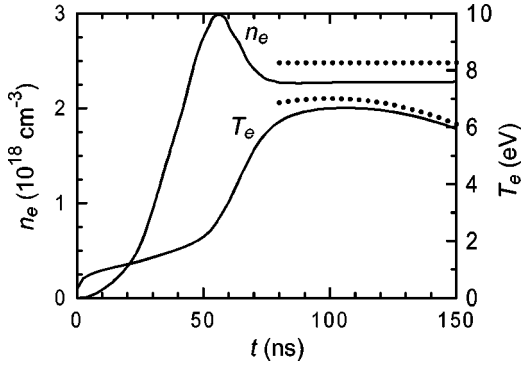

FIG. 2. Calculated temporal evolution of the axial electron density n_e and temperature T_e. The dotted lines show the results obtained with the simple model described in Sec. IV.

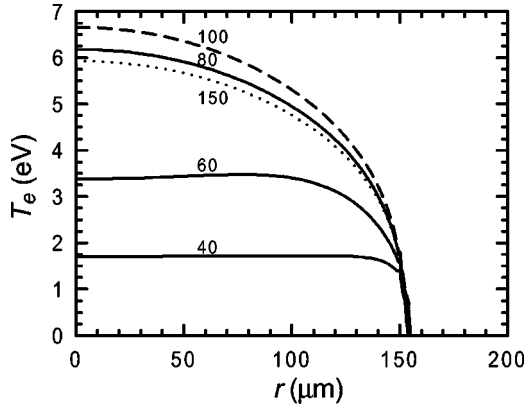

FIG. 4. Calculated radial profiles of electron temperature T_e for the same values of t as in Fig. 3.

this reason the radial distribution of plasma parameters corresponds to a quasi-steady-state equilibrium at a given electric current. This radial steady-state equilibrium indicates that the plasma pressure is almost homogeneous due to the condition $\beta \gg 1$. The plasma temperature at this stage has its maximum on the axis, as a consequence of the fact that cooling due to radiation plays a negligible role, and the Ohmic heating is balanced mainly by thermal conduction to the relatively cold capillary wall. Since the hydrogen is fully ionized and at constant pressure, a monotonic radially decreasing temperature results in an axial minimum in the electron density profile of the plasma.

The temporal evolution of the axial electron density and temperature are plotted in Fig. 2, showing that after $t \approx 80$ ns the axial electron density is constant. The axial electron temperature is found to decrease slowly with time after $t \approx 100$ ns. At $t \approx 60$ ns the electron density on the axis is $n_e \approx 2.8 \times 10^{18}$ cm^{-3} and the electron temperature is $T_e \approx 3.4$ eV.

The radial distributions of electron density and temperature at different moments of time are plotted in Figs. 3 and 4. An axial minimum in the radial electron density profile is established after about 65 ns, and indeed poor-quality channelling of radiation may be possible at $t \approx 60$ ns (see Fig. 3) owing to the steep rise in the electron density profile near the capillary wall. During the interval 80 ns$< t <$150 ns the radial distribution of electron density is almost constant—at least to the extent that longitudinal plasma flow may be neglected. The axial electron temperature reaches its maximum at the time of maximum electric current, thereafter decreasing slightly with time. The radial distribution of the electron temperature also changes only slightly within this time interval. If we do not take into account longitudinal plasma flow, the approximately parabolic electron density profile exists until the recombination of the hydrogen that occurs when the electron temperature becomes less than 1–2 eV [26,27].

In Fig. 5 we compare the measured and calculated electron density distributions for $t \approx 60$ ns. The electron density profile was obtained using laser pulses of approximately 8 ns duration, and by averaging several experimental curves recorded for t close to 60 ns. Hence the measured profiles correspond to an average of the electron density profile over several nanoseconds. The simulation shows that for $t \approx 60$ ns the electron density profile changes rapidly. Figure 5 also shows the calculated electron density profile for t

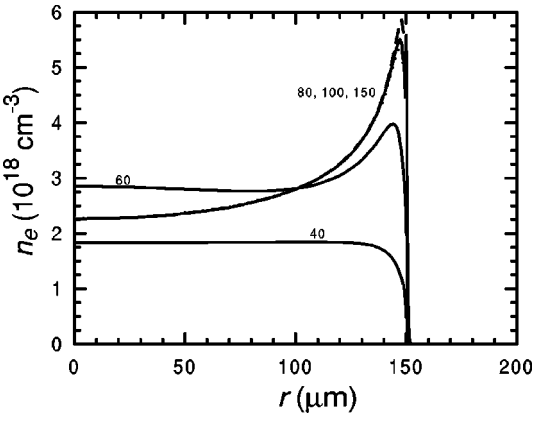

FIG. 3. Calculated radial electron density profiles n_e for $t = 40$, 60, 80, 100, and 150 ns. The curves are labeled by t in nanoseconds. The electron density profile is found to be almost constant in the interval 80 ns $< t <$ 150 ns, and the difference between the curves for $t = 80$ ns, 100 ns, and 150 ns is small.

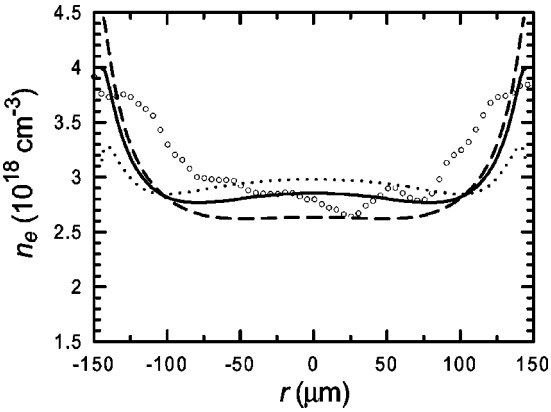

FIG. 5. Comparison of the simulated and measured electron density profiles. Open circles correspond to experimental results. The dotted line shows the electron density radial profile for $t = 55$ ns, the solid line for $t = 60$ ns, and the dashed line for $t = 65$ ns.

=55 ns and $t=65$ ns. It is seen that the measured electron density profile is reasonably well bracketed by these two simulations. We conclude, therefore, that allowing for errors in measurement of the time t of approximately ± 5 ns, and averaging over the duration of the probe pulse used in the measurements, the simulations are in good agreement with the measurements.

For practical applications of H-filled capillary discharge waveguides, it is important that the capillary has a long lifetime. The thermal flux due to electron thermal conduction penetrates the capillary wall, leading to partial ionization of the wall and heating of the free electrons. The lattice of the wall material is heated by energy exchange between these free electrons and the lattice. Our simulation shows that direct heating of the lattice due to ion-lattice thermal conduction plays only a secondary role in comparison with heating via free electrons in the wall material. For $t=100$–150 ns, the degree of ionization of atoms in the wall material is found to be of the order of 10^{-4} in a layer of ~ 0.8 μm depth. The electron temperature in this layer is of the order of 1.8 eV, whereas the lattice temperature grows from almost room temperature at $t=50$ ns to about 200 °C at $t=100$ ns and to about 500 °C at $t=150$ ns. Lattice temperatures of this magnitude do not lead to melting or disruption of the wall material. This finding agrees well with the experimental observation that after 10^5 discharge pulses the increase in capillary diameter was less than 1 μm [22].

IV. SIMPLE MODEL OF PLASMA EQUILIBRIUM INSIDE THE CAPILLARY CHANNEL

The results of the MHD simulation presented above show that, in contrast to previously discussed Z-pinch capillary waveguides, the pinch effect is insignificant under the conditions of the gas-filled capillary discharge waveguide. Furthermore, for $t \gtrsim 80$ ns the following conditions are found to be fulfilled. There is no screening of the axial electric field, and consequently it is uniform across the diameter of the capillary. The magnetic field pressure is much less than the plasma pressure (50–100 times less in the present simulation), and hence the plasma pressure can be considered to be constant across the capillary. The electrons are unmagnetized ($x_e \lesssim 0.04$), and consequently the influence of Nernst and Ettinghausen effects [see Eqs. (8) and (9)] can be neglected (i.e., we may let $\mathcal{N} \to 0$). There is no difference between electron T_e and ion T_i temperatures. As a result of these conditions, the distribution of plasma inside the capillary is simply determined by the balance between Ohmic heating, and cooling due to electron heat conduction. This allows us to formulate a simple model of the plasma under such equilibrium conditions.

First, we introduce a plasma temperature $T=T_i=T_e$. To obtain the radial profile of the plasma temperature we start from the equation for heat flow

$$\frac{1}{r}\frac{d}{dr}\left(r\kappa_{e\perp}\frac{dT}{dr}\right)+\sigma_\perp E^2=0, \tag{22}$$

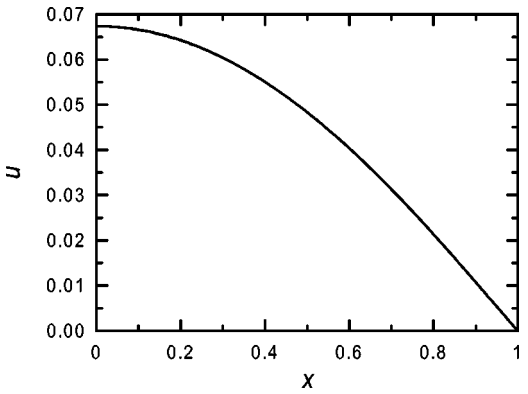

FIG. 6. The numerical solution of Eq. (25).

where $\kappa_{e\perp}$ is the electron thermal conductivity, and $\sigma_\perp$ is the electric conductivity, given by expressions (11) and (12), respectively. Equation (22) is a nonlinear ordinary differential equation, the boundary conditions in this case being

$$\left.\frac{dT}{dr}\right|_{r=0}=0, \quad T|_{r=R_0}=T^*, \tag{23}$$

where T^* is equal to the temperature of the wall. We may further simplify this equation as follows. Assuming the Coulomb logarithms to be constant (they are between 3 and 4 in the presented simulation), the electron thermal conductivity, and the electric conductivity vary as $\kappa_{e\perp}=\kappa_0 T^{5/2}$ and $\sigma_\perp=\sigma_0 T^{3/2}$, where κ_0 and σ_0 are constant values. Assuming that $\kappa_{e\perp}T|_{r=0} \gg \kappa_{e\perp}|_{r=R_0}T_*$ (in the case under consideration $\kappa_{e\perp}T|_{r=R_0} \approx 100\kappa_{e\perp}T|_{r=0}$), the temperature T^* in the boundary condition (23) at $r=R_0$ can be considered to be zero.

Introducing a new variable $\xi=r/R_0$ and a new function $u(\xi)$, which is related to the temperature by

$$T(\xi)=Au(\xi)^{2/7}, \tag{24}$$

with $A=(7\sigma_0 R_0^2 E^2/2\kappa_0)^{1/2}$, we may rewrite Eq. (22) in the form

$$\frac{1}{\xi}\frac{d}{d\xi}\left(\xi\frac{du}{d\xi}\right)=-u^{3/7}, \tag{25}$$

and the boundary conditions (23) as

$$\left.\frac{du}{d\xi}\right|_{\xi=0}=0, \quad u|_{\xi=1}=0. \tag{26}$$

The unique nontrivial solution of Eq. (25) with the boundary conditions (26) is found numerically and presented in Fig. 6. As discussed below, for further analysis we need to know the following three parameters of the solution: $u(0) \approx 0.067$, $u'(1) \approx -0.107$, and

$$m_0=\int_0^1 \xi u^{-2/7}(\xi)\,d\xi \approx 1.55. \tag{27}$$

As we already mentioned above, we suppose that the pressure p is constant across the capillary, so that in the case of full ionization $z \approx 1$,

$$p = 2n_e(r)T(r) = 2n_e(0)T(0), \tag{28}$$

where $n_e(r)$ and $T(r)$ are the values of the electron density and temperature at radius r. The average electron density $\langle n_e \rangle$ is equal to

$$\langle n_e \rangle = \frac{1}{\pi R_0^2} \int_0^{R_0} n_e 2\pi r dr. \tag{29}$$

In the absence of longitudinal flow, it is related to the initial ion density n_{i0} by, $\langle n_e \rangle = z n_{i0}$, where z is the degree of ionization. The electron density profile is given by

$$n_e(r) = \frac{n_e(0)T(0)}{T(r)} = n_e(0)\left(\frac{u(0)}{u(r)}\right)^{2/7}. \tag{30}$$

Substitution of the electron density profile into Eq. (29) then yields

$$\frac{n_e(0)}{\langle n_e \rangle} = \frac{1}{2m_0 u(0)^{2/7}} \approx 0.7364. \tag{31}$$

We see that the axial electron density is determined only by the average electron density, which in the absence of longitudinal flow is determined by the initial ion density and the degree of ionization z. For the case under consideration we find $n_e(0) \approx 2.5 \times 10^{18}$ cm^{-3}.

Expanding the solution for $u(\xi)$ we find

$$u(\xi) = u(0) + \frac{1}{2}\left.\frac{d^2u}{d\xi^2}\right|_{\xi=0} \xi^2 + \cdots = u(0)\left(1 - \frac{1}{4u(0)^{4/7}}\xi^2 + \cdots\right), \tag{32}$$

and hence the radial profile of the electron density becomes

$$\frac{n_e(r)}{n_e(0)} = \left(1 + \frac{1}{14u(0)^{4/7}}\frac{r^2}{R_0^2} + \cdots\right) \approx \left(1 + 0.33\frac{r^2}{R_0^2} + \cdots\right). \tag{33}$$

We see that near the capillary axis the electron density profile is approximately parabolic, which, as discussed below, allows laser pulses with a Gaussian transverse spatial profile to be matched to the plasma channel.

The electric field may be calculated as follows. The total electric current is given by

$$I = 2\pi \int_0^{R_0} j r dr = 2\pi\sigma_0 E \int_0^{R_0} T^{3/2} r dr, \tag{34}$$

where the electric current density is equal to $j = \sigma_\perp E$. Substitution of T from Eq. (24) and integration of Eq. (25) then yields,

$$I = 2\pi R_0^2 E A^{3/2} \sigma_0 \int_0^1 u^{3/7}(\xi)\xi d\xi = 2\pi R_0^2 E A^{3/2} \sigma_0 |u'(1)|. \tag{35}$$

This result may be used to write E in the form

$$E = \frac{1}{7^{3/10} 2^{1/10} \pi^{2/5} |u'(1)|^{2/5}} \frac{\kappa_0^{3/10}}{\sigma_0^{7/10}} \frac{I^{2/5}}{R_0^{7/5}}, \tag{36}$$

or

$$E \ [\text{kV cm}^{-1}] \approx 0.085 \frac{I \ [\text{kA}]^{2/5}}{R_0 \ [\text{mm}]^{7/5}}. \tag{37}$$

The resistance $\mathcal{R}$ per unit length of the plasma may be found from $E = I\mathcal{R}$ and is equal to

$$\mathcal{R} \ [\text{ohm cm}^{-1}] \approx 0.085 I \ [\text{kA}]^{-3/5} R_0 \ [\text{mm}]^{-7/5}. \tag{38}$$

Equation (24) then gives the temperature on the axis as

$$T(0) = \frac{7^{1/5} u(0)^{2/7}}{2^{3/5}\pi^{2/5}|u'(1)|^{2/5}} \frac{1}{(\kappa_0\sigma_0)^{1/5}} \left(\frac{I}{R_0}\right)^{2/5} \approx 5.7 \left(\frac{I \ [\text{kA}]}{R_0 \ [\text{mm}]}\right)^{2/5} \text{eV}. \tag{39}$$

The numerical coefficients in Eqs. (37) and (39) have been calculated for $\lambda_{ee} \approx 4.4$, $\lambda_{ei} \approx 4.7$, $z \approx 1$, $w \approx 0.66$, $\Gamma_1 \approx 3.33$, and $\Gamma_5 \approx 0.50$. These values are calculated using the simulated plasma parameters at the axis for $t = 100$ ns, and are assumed to be constant.

We see that the equilibrium state of the capillary discharge depends, assuming full ionization of the hydrogen, only on the electric current, the capillary radius, and the total mass of hydrogen per unit length of the capillary. We can consider the quasi-steady-state development of the capillary discharge as an evolution of such equilibrium states as the electric current changes with time. Within this picture the axial temperature depends on the electric current, and consequently changes as the discharge evolves. However, the axial electron density does not depend on electric current, and hence is constant in time to the extent that z is constant. The calculated temporal evolution of the axial electron density and temperature according to Eqs. (31) and (39) are shown by dotted lines in Fig. 2, assuming $z \approx 1$. It can be seen that after $t \gtrsim 80$ ns, for both parameters the differences between the MHD simulation and the simple model become less than about 10%. In Fig. 7 we compare the calculated radial profiles of the electron temperature and density for the MHD simulation and the equilibrium model at $t = 100$ ns. The agreement of the simple model with the MHD simulations is quite acceptable.

Both the MHD and equilibrium simulations were performed within a one-dimensional approximation in which the plasma outflow in the z direction through the ends of the capillary is not taken into account. We now estimate the ef-

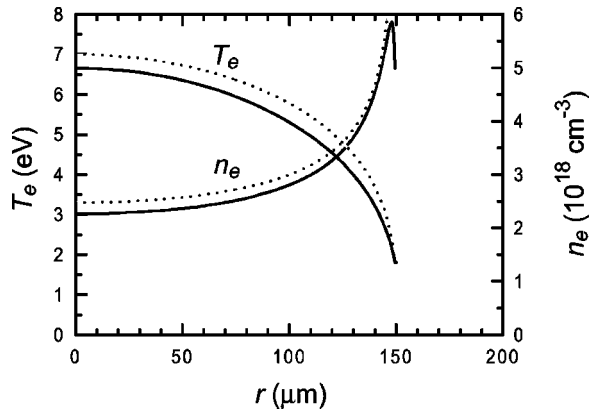

FIG. 7. Comparison of the simulated electron density and temperature profiles (solid lines) with those calculated from the simple model described in Sec. IV (dotted lines). For both calculations $t = 100$ ns.

fect of longitudinal plasma flow using a simple model. We assume that the velocity of plasma along the capillary axis is proportional to the z coordinate, i.e., $v_z = z/\tau$, where $\tau = l/c_s$, and $c_s = \sqrt{T_e/m_i}$ is the ion acoustic velocity. Then from the continuity equation we have

$$\frac{dn}{dt} + \frac{n}{\tau} = 0 \tag{40}$$

and

$$n = n_0 \exp(-t/\tau), \tag{41}$$

with τ being the time scale of outflow.

For 3–5 mm long capillaries, as used in the guiding experiments [22], once the hydrogen is fully ionized τ is calculated to be of the order of 150–250 ns. With this value of τ the time for the plasma density to decrease by an order of magnitude is estimated to be approximately 600 ns for a 5 mm long capillary. This agrees well with the experimental observation [22] that the plasma density inside a 5-mm long capillary decayed to zero in a time of order 650 ns. We conclude, therefore, that for the short capillaries employed in the measurements of the electron density profile, longitudinal plasma flow should not have affected the radial electron density profile for $t \lesssim 150$ ns. Further evidence for this is the good agreement between the measured and calculated profiles. The time scale of longitudinal flow is expected to increase approximately linearly with l, and hence for longer capillaries our simulations are is expected to be valid for much longer times.

For $t > 80$ ns the simple model can be used if the length of the capillary is such that the time-scale for longitudinal flow exceeds the skin and thermal conduction times. We note that for capillaries with lengths of interest for guiding, i.e., tens of millimetres, there exists a substantial window between the formation of a parabolic guiding channel at $t \approx 80$ ns and the onset of longitudinal plasma flow. For example, in recent guiding experiments [28] with a 20-mm long H-filled capillary discharge waveguide, high-quality guiding of intense laser pulses was observed in the region near $t = 200$ ns. Longitudinal flow would not be expected to occur for this capillary until $t \approx 1$ μs.

V. LASER PULSE GUIDING INSIDE THE CAPILLARY

A Gaussian beam will propagate through a plasma channel with a parabolic electron density profile of the form $n_e(r) = n_e(0) + n_e''(0) r^2/2$ with a constant spot size W_M provided that

$$W_M = (\lambda R_0)^{1/2} \left(\frac{n_{cr}}{2\pi^2 n_e(0)} \right)^{1/4} \left(\frac{n_e(0)}{n_e''(0) R_0^2} \right)^{1/4}. \tag{42}$$

Equation (42) can also be written in the form

$$W_M = \left(\frac{2}{\pi r_e n_e''(0)} \right)^{1/4}, \tag{43}$$

where r_e is the classical electron radius, which shows more clearly that the matched spot size does not depend on λ. From the equilibrium model presented above we find that the matched spot size is given by

$$W_M = [28 m_0 u(0)^{6/7}]^{1/4} \left(\frac{R_0^2}{\pi r_e z n_{i0}} \right)^{1/4}. \tag{44}$$

We note that although the electron density profile is not exactly parabolic, for the purposes of matched guiding it is sufficient that the profile is approximately parabolic for $r \lesssim 2 W_M$, at which point the intensity of the guided beam is reduced from the axial value by a factor of almost 10^4. This condition is well satisfied for the device discussed here.

Using the values $u(0) \approx 0.067$, $m_0 \approx 1.55$, we find

$$W_M \ [\mu\text{m}] \approx 1.48 \times 10^5 \frac{\sqrt{R_0 \ [\mu\text{m}]}}{(z n_{i0} \ [\text{cm}^{-3}])^{1/4}} \tag{45}$$

and we see that the matched spot size is proportional to the square root of the capillary radius, but depends only slightly on the initial gas pressure and the degree of ionization. Taking $R_0 = 150$ μm and an initial hydrogen pressure of 67 mbar, we find that $W_M \approx 42$ μm, which is in good agreement with the value of 37.5 μm determined from a parabolic fit to the measured electron density profile [22]. We note that it should be possible to generate plasma channels with smaller matched spot sizes by employing capillaries of smaller diameter.

VI. CONCLUSION

We have employed a one-dimensional dissipative MHD code to investigate the dynamics of hydrogen-filled capillary discharge waveguide under the conditions described in Refs. [22,28]. We have found that the evolution of the discharge in this device is substantially different compared with the discharge dynamics in the discharge-ablated and *Z*-pinch capillary discharges discussed in Refs. [25,26,29–31,20,34].

We have shown that the main reason for this difference is

that in the hydrogen-filled capillary discharge waveguide the plasma pressure is always much greater than the magnetic pressure, and as such the pinch effect can be neglected. In this case radial expansion of the capillary plasma is restricted by the elasticity and inertia of the capillary walls.

Three stages of the plasma evolution have been identified. During the first stage the magnetic field penetrates the plasma on a time scale of $\sim$1 ns, and the plasma is heated and ionized locally. Radial distributions of the plasma parameters remain homogeneous. As the electric current increases the thermal conduction time decreases, and thermal conduction becomes significant at approximately the time of complete ionization of the plasma. A redistribution of the plasma temperature and density across the channel occurs during this second stage of the discharge evolution. In the third stage the discharge plasma is in dynamic and thermal quasiequilibrium. During this phase the plasma pressure is uniform, and the electron density profile is approximately parabolic with a minimum on the axis, where the plasma temperature is maximum.

We have compared the results of the MHD simulations of the electron density profile with those measured in a recent experiment, and found good agreement. The plasma channel is shown to be fully ionized, which is important for applications of the waveguide in that pulse distortion and spectral blue-shifting due to laser-induced ionization of the plasma will be avoided. Furthermore, the simulations show that the capillary wall is not significantly ablated by the discharge pulse, which is in agreement with the long device lifetime found experimentally.

The results of the MHD simulation allowed us to formulate a simple model to determine the plasma temperature and density during the third stage of the discharge, in which the distribution of plasma inside the capillary is determined by the balance between ohmic heating and cooling due to electron heat conduction. We have presented the unique solution for the temperature profile within the capillary, and found scaling laws for the dependence of the axial plasma temperature and electron density. The results of this simple model were shown to be in good agreement with the MHD simulations. The key advantages of the simple model are that it provides analytical expressions, in terms of the parameters of the capillary discharge, for both the plasma distribution inside the capillary, and the matched spot size of the plasma channel that is formed.

ACKNOWLEDGMENTS

This work was supported in part by the Engineering and Physical Sciences Research Council (EPSRC) of the United Kingdom, through Grant No. GR/M88969 and assistance for D. J. Spence and A. Butler. S. M. Hooker would like to thank the Royal Society for support. The work was also supported by RFBR through Grant No. 00-02-16635.

[1] C. J. Joshi and P. B. Corkum, Physics Today **48**(1), 36 (1995).
[2] T. Tajima and J. M. Dawson, Phys. Rev. Lett. **43**, 267 (1979).
[3] A. Modena, Z. J. Najmudin, and A. E. Dangor, *et al.*, Nature (London) **337**, 606 (1995).
[4] K. Nakajima, D. Fisher, and T. Kawakubo, *et al.*, Phys. Rev. Lett. **74**, 4428 (1995).
[5] T. Tajima, Laser Part. Beams **3**, 1432 (1985); P. Sprangle *et al.*, Phys. Rev. A **41**, 4463 (1990); S. V. Bulanov, F. F. Kamenets, F. Pegoraro, and A. M. Pukhov, Phys. Lett. A **195**, 84 (1994); C. G. Durfee III, J. Lynch, and H. M. Milchberg, Phys. Rev. E **51**, 2368 (1995); T. C. Chou, T. Katsouleas, C. D. Decker, W. B. Mori, J. S. Wurtele, G. Shvets, and J. J. Su, Phys. Plasmas **2**, 310 (1995).
[6] P. Monot, T. Auguste, P. Gibbon, F. Jakober, G. Mainfray, A. Dulieu, M. Louis-Jacquet, G. Malka, and J. L. Miquel, Phys. Rev. Lett. **74**, 2953 (1995).
[7] A. B. Borisov, A. V. Borovskiy, V. V. Korobkin, A. M. Prokhorov, O. B. Shiryaev, X. M. Shi, T. S. Luk, A. McPherson, J. C. Solem, K. Boyer, and C. K. Rhodes, Phys. Rev. Lett. **68**, 2309 (1992).
[8] S. Jackel, R. Burris, J. Grun, A. Ting, C. Manka, K. Evans, and J. Kosakowskii, Opt. Lett. **20**, 1086 (1995).
[9] F. Dorchies, J. R. Marques, B. Cros, G. Matthieussent, C. Courtois, T. Velikoroussov, P. Audebert, J. P. Geindre, S. Rebibo, G. Hamoniaux, and F. Amiranoff, Phys. Rev. Lett. **82**, 4655 (1999).
[10] C. Courtois, B. Cros, G. Malka, G. Matthieussent, J. R. Marques, N. Blanchot, and J. L. Miquel, J. Opt. Soc. Am. B **17**, 864 (2000).
[11] C. G. Durfee III and H. M. Milchberg, Phys. Rev. Lett. **71**, 2409 (1993).
[12] S. P. Nikitin, I. Alexeev, J. Fan, and H. M. Milchberg, Phys. Rev. E **59**, R3839 (1999).
[13] P. Volfbeyn, E. Esarey, and W. P. Leemans, Phys. Plasmas **6**, 2269 (1999).
[14] J. Fan, E. Parra, I. Alexeev, K. Y. Kim, H. M. Milchberg, L. Y. Margolin, and L. N. Pyatnitskii, Phys. Rev. E **62**, R7603 (2000).
[15] Y. Ehrlich, C. Cohen, A. Zigler, J. Krall, P. Sprangle, and E. Esarey, Phys. Rev. Lett. **77**, 4186 (1996).
[16] D. Kaganovich, A. Ting, C. I. Moore, A. Zigler, H. R. Burris, Y. Ehrlich, R. Hubbard, and P. Sprangle, Phys. Rev. E **59**, R4769 (1999).
[17] S. M. Hooker, D. J. Spence, and R. A. Smith, J. Opt. Soc. Am. B **17**, 90 (2000).
[18] T. Hosokai, M. Kando, H. Dewa, H. Kotaki, S. Kondo, N. Hasegawa, K. Nakajima, and K. Horioka, Opt. Lett. **25**, 10 (2000).
[19] C. Fauser and H. Langhoff, Appl. Phys. B: Lasers Opt. **71**, 607 (2000).
[20] M. C. Marconi, C. H. Moreno, J. J. Rocca, V. N. Shlyaptsev, and A. L. Osterheld, Phys. Rev. E **62**, 7209 (2000).
[21] B. Cros, C. Courtois, G. Malka, G. Matthieussent, J. R. Marques, F. Dorchies, F. Amiranoff, S. Rebibo, G. Hamoniaux, N. Blanchot, and J. L. Miquel, IEEE Trans. Plasma Sci. **28**, 1071 (2000).
[22] D. J. Spence and S. M. Hooker, Phys. Rev. E **63**, 015401(R) (2001).

[23] Y. Ehrlich, C. Cohen, D. Kaganovich, A. Zigler, R. F. Hubbard, P. Sprangle, and E. Esarey, J. Opt. Soc. Am. B **15**, 2416 (1998).
[24] D. J. Spence, P. D. S. Burnett, and S. M. Hooker, Opt. Lett. **24**, 993 (1999).
[25] N. A. Bobrova, S. V. Bulanov, D. Farina, R. Pozzoli, T. L. Razinkova, J.-I. Sakai, and P. V. Sasorov, J. Phys. Soc. Jpn. **67**, 3437 (1998).
[26] N. A. Bobrova, S. V. Bulanov, A. A. Esaulov, and P. V. Sasorov, Plasma Phys. Rep. **26**, 12 (2000).
[27] N. A. Bobrova, S. V. Bulanov, D. Farina, R. Pozzoli, T. L. Razinkova, J.-I. Sakai, P. V. Sasorov, and I. V. Sokolov, Laser Part. Beams **18**, 623 (2000).
[28] D. J. Spence, A. Butler, and S. M. Hooker, J. Phys. B **34**, 4103 (2001).
[29] N. A. Bobrova, S. V. Bulanov, T. L. Razinkova, and P. V. Sasorov, Plasma Phys. Rep. **22**, 349 (1996).
[30] N. A. Bobrova, S. V. Bulanov, D. Farina, R. Pozzoli, T. L. Razinkova, and P. V. Sasorov, Plasma Phys. Rep. **24**, 1 (1998).
[31] D. Kaganovich, P. Sasorov, C. Cohen, and A. Zigler, Appl. Phys. Lett. **75**, 772 (1999).
[32] N. A. Bobrova and P. V. Sasorov, Plasma Phys. Rep. **19**, 409 (1993).
[33] S. I. Braginskii, *Reviews of Plasma Physics*, edited by M. A. Leontovich (Consultants Bureau, New York, 1963), Vol. 1.
[34] A. Esaulov, P. Sasorov, L. Soto, M. Zambra, and J.-I. Sakai, Plasma Phys. Controlled Fusion **43**, 571 (2001).
[35] L. D. Landau, and E. M. Lifshitz, *Electrodynamics of Continuous Media* (Pergamon Press, Oxford, 1960).
[36] Boart Longyer Catalogue and the CRC Handbook of Chemistry and Physics (CRC Press, Boca Raton, FL, 1995), Sec. 12, p. 179.
[37] Ya. B. Zeldovich and Yu. P. Raizer, *Physics of Shock Waves and High-Temperature Hydrodynamic Phenomena* (Academic Press, New York, 1967).
[38] S. I. Braginskii, JETP **33**, 645 (1957).
[39] R. S. Pease, Proc. R. Soc. London **70**, 45 (1957).
[40] N. A. Bobrova, T. L. Razinkova, and P. V. Sasorov, Plasma Phys. Rep. **18**, 263 (1992).
[41] V. V. Aleksandrov, A. V. Branitskii, G. S. Volkov, E. V. Grabovskii, M. V. Zurin, S. L. Nedoseev, G. M. Oleinik, A. A. Samokhin, P. V. Sasorov, V. P. Smirnov, M. V. Fedulov, and I. N. Frolov, Plasma Phys. Rep. **27**, 89 (2001).
[42] A. A. Esaulov, P. V. Sasorov, L. Soto, and M. Zambra, Phys. Plasmas **8**, 1395 (2001).